Journal of Molecular Graphics and Modelling 84 (2018) 236–241

Contents lists available at ScienceDirect

Journal of Molecular Graphics and Modelling

journal homepage: www.elsevier.com/locate/JMGM

Molecular dynamics simulations suggest changes in electrostatic interactions as a potential mechanism through which serine phosphorylation inhibits DNA polymerase β activity☆

Dirar Homouz [a, b, c], Kwee Hong Joyce-Tan [d], Mohd ShahirShamsir [d], Ibrahim M. Moustafa [e], Haitham T. Idriss [f, *, 1]

[a] Department of Statistics and Applied Mathematics Khalifa University, Abu Dhabi, United Arab Emirates
[b] Department of Physics, University of Houston, Houston, TX, USA
[c] Center for Theoretical Biological Physics, Rice University, Houston, TX, USA
[d] Faculty of Bioscience and Bioengineering, Universiti Teknologi Malaysia, Johor, Malaysia
[e] Department of Chemistry, Bowdoin College, Maine, USA
[f] Department of Biology and Biochemistry, Birzeit University, Palestine

ARTICLE INFO

Article history:
Available online 14 August 2018

ABSTRACT

DNA polymerase β is a 39 kDa enzyme that is a major component of Base Excision Repair in human cells. The enzyme comprises two major domains, a 31 kDa domain responsible for the polymerase activity and an 8 kDa domain, which bind ssDNA and has a deoxyribose phosphate (dRP) lyase activity. DNA polymerase β was shown to be phosphorylated *in vitro* with protein kinase C (PKC) at serines 44 and 55 (S44 and S55), resulting in loss of its polymerase enzymic activity, but not its ability to bind ssDNA. In this study, we investigate the potential phosphorylation-induced structural changes for DNA polymerase β using molecular dynamics simulations. The simulations show drastic conformational changes of the polymerase structure as a result of S44 phosphorylation. Phosphorylation-induced conformational changes transform the closed (active) enzyme structure into an open one. Further analysis of the results points to a key hydrogen bond and newly formed salt bridges as potential drivers of these structural fluctuations. The changes observed with S55/44 and S55 phosphorylation were less dramatic and the integrity of the H-bond was not compromised. Thus the phosphorylation of S44 is the major contributor to structural fluctuations that lead to loss of enzymatic activity.

1. Introduction

DNA stability ($t_{1/2} = 30$ million years) inside cells is undermined by susceptibility to damage by various agents such as nucleophiles (free radicals) or through malfunctioning of DNA-binding enzymes (e.g. polymerases, ligases or topoisomerases) [1]. Cellular DNA experiences various insults during a cell's lifespan resulting in DNA damage (at about 7 lesions/cell/minute) [1]. Physical, chemical and/or biological insults result in a number (about fifteen different types) of observed DNA damage including fragmentation, deletion, nucleotide or base substitution [1]. The consequences of such damage lead to defective or inaccurate gene replication resulting in abnormal cell function and disease [1]. If not repaired, DNA damage leads to either cell death (e.g. degenerative neurological disorders) or mutations causing uncontrolled cell proliferation (as seen in cancer) [1]. The DNA repair machinery is a mechanism utilized by the cell to correct DNA damage. This repair machinery consists of different types of repair such as base excision repair, single and double-strand break repair [1]. Each type of repair consists of several key proteins performing correction function. DNA repair proteins are potential targets for therapeutic interventions [2]. DNA polymerase β is a key component of Base Excision Repair (BER). The enzyme performs the distributive polymerase gap-filling function as well as deoxyribose phosphate (dRP) lyase activity [3].

DOI of original article: https://doi.org/10.1016/j.jmgm.2017.11.002.
☆ This article first appeared in volume 79, please see publisher's note: https://doi.org/10.1016/j.jmgm.2017.11.002.
* Corresponding author.
E-mail addresses: hidriss@birzeit.edu, haitham@annalqudsmed.com, idriss@ic4life.net (H.T. Idriss).
[1] Annals of AlQudsMedicine (www.annalqudsmed.com).

https://doi.org/10.1016/j.jmgm.2018.08.007
1093-3263/

DNA polymerase β is a 39 kDa enzyme that comprises two major domains, a 31 kDa domain responsible for the polymerase activity and an 8 kDa domain, which bind ss DNA and has the dRP lyase activity [3]. The atomic structure has previously been elucidated and several crystal structures have since been published for the enzyme and its binary and ternary complexes ([4–6]). Key features of DNA polymerase β's structure suggest its organization in three major structural sub-domains: C (catalytic), D (DNA binding), N (nascent base pair binding) [4,5] (see Fig. 1). These three sub-domains correspond to the palm, thumb, and fingers sub-domains, which were observed for other polymerases such as HIV-1 reverse transcriptase [6]. Each of these three structural sub-domains serves a specific function with the palm serving as the platform that holds the DNA template-primer, whilst palm and fingers align template/primer towards polymerase active site. DNA polymerase β was shown to be phosphorylated *in vitro* with protein kinase C (PKC) at S44 and 55, resulting in loss of its polymerase enzymatic activity, but not its ability to bind ssDNA [7]. The enzyme was also observed to be phosphorylated *in vivo* in HeLa cells nuclei (Idriss, H, Kumar A and Wilson SH, unpublished observation), although this has not been conclusively reproduced. Several DNA polymerases are regulated through reversible post-translational modifications and DNA polymerase β was shown to be post-translationally phosphorylated, acetylated and methylated with functional consequences [7–10].

Since PKC phosphorylation affects DNA Polymerase β's polymerase activity, we argued that phosphorylation should also alter the enzyme's structure, as well as its overall charge. Therefore, we set out to simulate potential phosphorylation-induced structural changes for DNA polymerase beta using molecular modeling force field (CHARMM22) and published structural coordinates (pdb: 2FMS, 3ISB, and 1BPD). Other computational studies exist that looked at various aspects of the enzyme's structure/function [11–13].

2. Objectives

- Molecular dynamics simulation of DNA polymerase β in its apo state and its phosphorylated structure at S44, S55, and S44/55.
- Structural and dynamics study of DNA polymerase β and its phosphorylated structure via MD simulation.

3. Methodology

The X-ray crystal structures of DNA polymerase β (PDB entries: 2FMS [14], 3ISB [15], and 1BPD [16]) were downloaded from PDB. 2FMS is the ternary complex (human DNA polymerase β), 3ISB is the binary complex (human DNA polymerase β), and 1BPD is free DNA polymerase β (rat). Coordinates of the DNA substrate and dUMPNPP in 2FMS were removed to yield a structure which only contains the protein. Using this DNA polymerase β structure, separate structures with (1) S44 (pS44), (2) S55 (pS55), (3) S44 and S55 (pS4455) phosphorylated respectively were built using VMD [17]. Topology needed to patch the phosphorylated residues were added into the CHARMM22 [18] all-hydrogen topology file for protein accordingly. The phosphorylated serine residue was modeled using the SP2 phosphoserine patch from the toppar stream files which are part of the CHARMM22. The modeled structures did not include the magnesium ions Mg^{2+}.

The free energy landscape estimation was performed using the Boltzmann inversion method. Finally, the cluster analysis was done using a method based on self-organized neural net algorithm [19,20]. In this clustering analysis, each confirmation is represented by a feature vector that is used to partition all conformations into different clusters. Each cluster is specified by its center and size (radius). A conformation is assigned a specific cluster if its distance to the center is smaller than a pre-set threshold value. The algorithm has two phases, the learning phase in which the centers of clusters are learned and the refining phase in which conformations are reassigned to the correct clusters. For further details of this method, we refer the reader to [21]. The clustering analysis in this work uses a feature vector whose elements is the pairs of side chain native contacts (calculated using DSSP program [22]).

3.1. System setup for molecular dynamics simulations

All the MD simulations were performed with NAMD 2.7 [23] program using the CHARMM22 force field and the TIP3P water model [24]. Force field parameter needed for patching the phosphorylated residues were added accordingly. Counter ions were added accordingly to neutralize the systems. Langevin dynamics with a Langevin damping coefficient of $5ps^{-1}$ was used to keep all the non-hydrogen atoms in the simulated systems at 300 K; Langevin dynamics control the temperature by introducing additional damping and random forces. Nosé-Hoover Langevin piston [25] was used to maintain the pressure of the simulated systems at

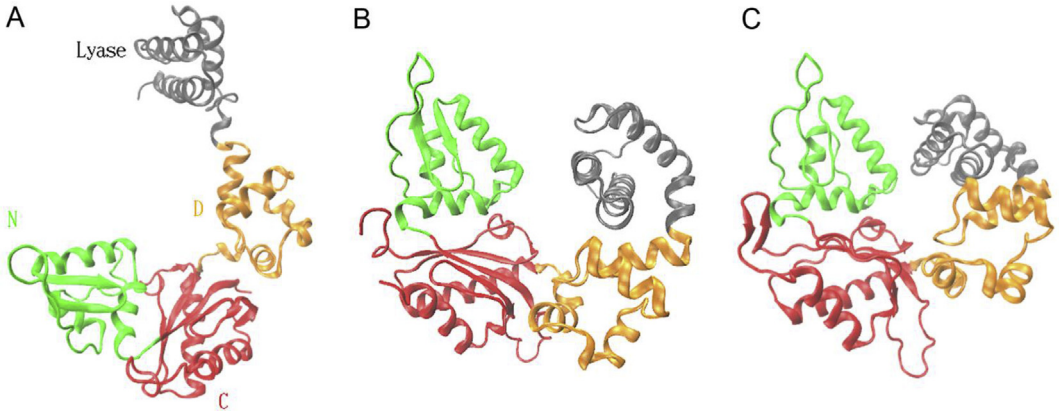

Fig. 1. (A) The structure of extended DNA polymerase β (PDB entry: 1BPD). The major feature of the structure includes the Lyase domain (grey) in addition to the polymerase domain with its three sub-domains: DNA binding (D, residues 90–150) (orange), catalytic (C, residues 151–260) (red), and nascent base pair binding (N, residues 261–335) (green). (B) The structure of open DNA polymerase β (PDB entry: 3ISB) with the same color scheme in (A). (C) The structure of closed DNA polymerase β (PDB entry: 2FMS) with the same color scheme in (A). (For interpretation of the references to color in this figure legend, the reader is referred to the Web version of this article.)

1 atm with a period of 100 fs and damping timescale of 50fs The integration time step of the simulations was set at 2 fs under a multiple time stepping scheme where bonded interactions were computed every time step while non-bonded interactions were computed every two time-steps. The cutoff for the van der Waals and short-range electrostatic interactions were set at 12 Å with the switching function set at 10 Å to ensure a smooth cut-off for the van der Waals interactions. The simulations were performed under periodic boundary conditions using the Particle Mesh Ewald (PME) algorithm [26,27].

The systems were first minimized 1000 steps using the conjugate-gradient method with the protein backbone held fixed, followed by a 1000-steps-minimization. Then the temperature of the systems was gradually increased to 300 K in 6 ps while restraining the protein backbone before the equilibration took place. In the equilibration process, the system was first equilibrated for 20 ps with protein backbone restrained then the protein backbone was released to allow the system to be equilibrated for another 200–400 ps. The production dynamics were then performed for 100 ns at the time step of 2fs All the resulting 100ns trajectories were analyzed using VMD utilities and additional TCL scripts.

4. Result and discussion

DNA polymerase β assumes several intermediate structures along its reaction pathways [5]. The unliganded enzyme has an extended structure (1BPD, see Fig. 1A). It adopts a doughnut-like open structure after binding DNA (3ISB, see Fig. 1B) which undergoes further conformational changes to the closed structure after binding dNTP (2FMS, see Fig. 1C). In this work, we studied the effects of phosphorylation on the enzyme using MD simulations of several systems. The systems include five 2FMS systems: unphosphorylated 2FMS (apo-2FMS), S44 phosphorylated 2FMS (pS44-2FMS), S55 phosphorylated (pS55-2FMS), S44 and S55 phosphorylated 2FMS (pS44-pS55-2FMS) and S44 to D44 mutated 2FMS (S44D-2FMS). We also simulated four 3ISB systems: (apo-3ISB), (pS44-3ISB), (pS55-3ISB), and (pS44-pS55-3ISB). In addition, one phosphorylated 1BPD system (pS44-pS55-1BPD) was simulated for comparison, since biochemical studies were performed using rat DNA polymerase [7] and we used human DNA polymerase for molecular dynamics.

4.1. S44 phosphorylation induces major structural fluctuations

In order to assess structural changes of the enzyme in our simulations, we calculated the root mean square deviation (RMSD) of each structure from their respective initial coordinates as a function of time where each frame saved during the simulation was compared to the initial structure (The time evolution of C_α-RMSD is shown in Fig. S1). In addition, we analyzed the radius of gyration (R_g) of the protein backbone which measures the compactness of the protein as the function of time. These two parameters, RMSD and R_g, are used to calculate the two-dimensional free energy of the enzyme which is shown in Fig. 2.

Fig. 2A shows that the apo-2FMS structures fluctuate around a basin with average values μ_{RMSD} of 2.48 Å and μ_{Rg} of 22.3 Å. The spread of the basin around these average values is relatively small as measured by standard deviation ($\sigma_{RMSD} = 0.39$ Å, $\sigma_{Rg} = 0.17$ Å). Out of all studied phosphorylated systems, pS44 exhibits the biggest structural changes as seen in Fig. 2B. The pS44-2FMS conformations populate a much bigger area of the 2D free energy surface ($\sigma_{RMSD} = 0.93$ Å, $\sigma_{Rg} = 0.63$ Å) and shift to higher average values ($\mu_{RMSD} = 4.03$ Å, $\mu_{Rg} = 23.1$ Å) indicating large deviations of protein structure. The combined phosphorylation of S44 and S55 (Fig. 2C) leads to large deviations ($\mu_{RMSD} = 3.73$ Å, $\sigma_{RMSD} = 0.73$ Å) similar to pS44 however with smaller and less fluctuating size ($\mu_{Rg} = 22.2$ Å, $\sigma_{Rg} = 0.22$ Å). Interestingly, phosphorylating S55 (Fig. 2D) seems to stabilize the protein structure with smaller values of RMSD ($\mu_{RMSD} = 2.04$ Å, $\sigma_{RMSD} = 0.34$ Å) and small fluctuations in R_g ($\mu_{Rg} = 22.3$ Å, $\sigma_{Rg} = 0.28$ Å) in comparison with the apo-2FMS.

On the other hand, from Fig. 2E–H of free energy of the open structure 3ISB, we see that the two different phosphorylations (pS55 and pS44/55) induce smaller effects on the protein structure in comparison with pS44 in 2FMS. Moreover, the apo-3ISB has relatively large fluctuations in both RMSD and R_g due to the open nature of the structure which explains the small effect of phosphorylation.

In order to assess the convergence of the simulated systems, we calculated the number of transitions between the states shown in Fig. 2. Our calculations show that the simulated systems were not trapped in metastable states and they had access to other states. For each simulated system, the whole 100-ns second trajectory is used in free energy calculation. Each system was able to make thousands of transitions between possible states.

4.2. pS44-induced fluctuations open up 2FMS structure

Among the studied systems, phosphorylation at S44 had induced the greatest conformational changes in the closed 2FMS structure. In order to see the regions most affected by these changes, we calculated the root mean squared fluctuations (RMSF) for all protein residues. The RMSF value reflects the average fluctuation of each residue over the total time of the simulation. Fig. 3A compares the RMSF of pS44-2FMS with that of apo-2FMS which show that pS44 induces the highest excess fluctuations in the Lyase domain and the N-sub-domain. When the pS44-2FMS structure is aligned with that of apo-2FMS (Fig. 3B), we can see that most conformation changes happen are due to the repositioning of the N-sub-domain. The repositioning is characterized by a twist motion that separates the Lyase domain (grey) from N-sub-domain (green). This will lead the structure to open up which undermines the stability gained after binding dNTP [5] that caused 2FMS to close in the first place. It is interesting to see that pS44-2FMS structure is better aligned with open apo-3ISB than the closed apo-2FMS as can be seen in Fig. 3C.

4.3. Phosphorylating S44 disrupts S44-E335 H-bond

The experimental data derived from crystal structures indicate that the open binary DNA complex (3ISB) does not have H-bond between S44 and E335, but that the closed ternary complex (2FMS) does have this H-bond [14,15] (Fig. 4). Accordingly, this interaction would be expected to stabilize the closed polymerase conformation. To test the effect of phosphorylation of S44 on this bond we calculated the average donor-acceptor distance between S44 and E335 and the H-bond occupancy in all simulated systems. The results are summarized in Table 1. The results show S44 phosphorylation disrupts S44-E335 H-bond in all simulated system ($HB_{avg} = 0.0\%$). This total disruption is due to the negative charge on phosphate group. This is confirmed by the simulation results of phosphomimetic S44D mutant 2FMS which have zero average HB occupancy as well. Comparing apo-2FMS with apo-3ISB, we see that the open structure has a smaller HB occupancy. Moreover, the HB occupancy was calculated for the extended structure 1BPD and it is equal to zero. Thus, it is clear that disruption of this H-bond plays a very important role in opening up the structure of pS44 systems.

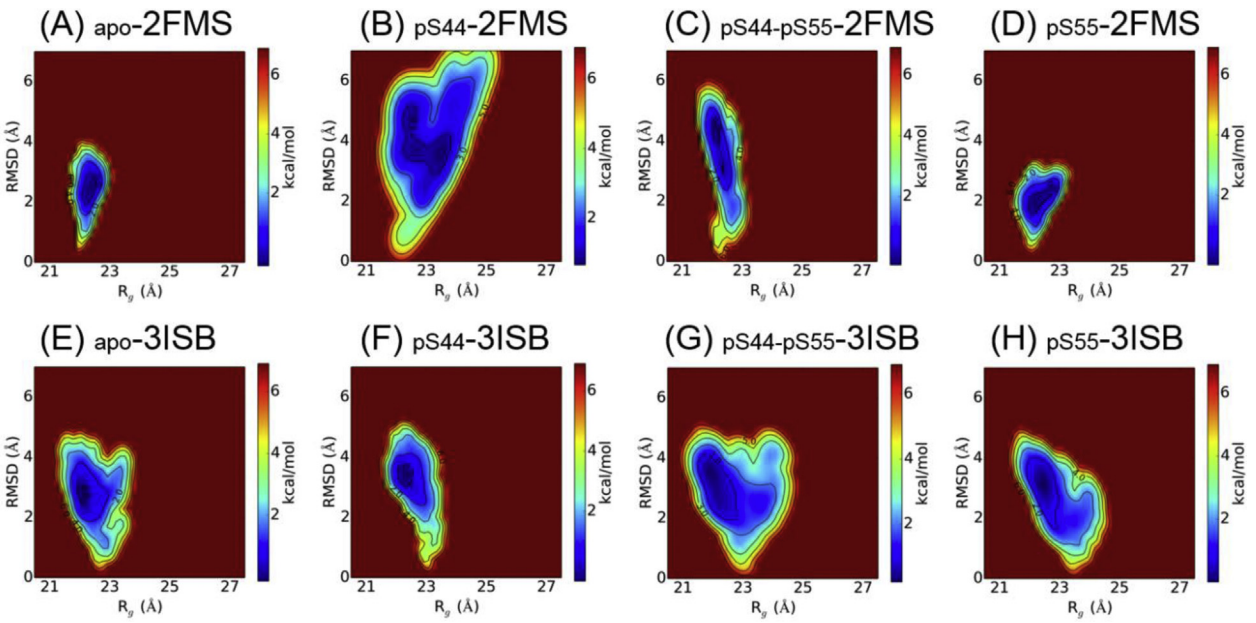

Fig. 2. The free energy (kcal/mol) for DNA polymerase β as a function of R_g (Å) and RMSD (Å) for (A) un-phosphorylated 2FMS, (B) S44 phosphorylated 2FMS, (C) S44-55 phosphorylated 2FMS, (D) S55 phosphorylated 2FMS, (E) un-phosphorylated 3ISB, (F) S44 phosphorylated 3ISB, (G) S44-55 phosphorylated 3ISB, and (H) S55 phosphorylated 3ISB.

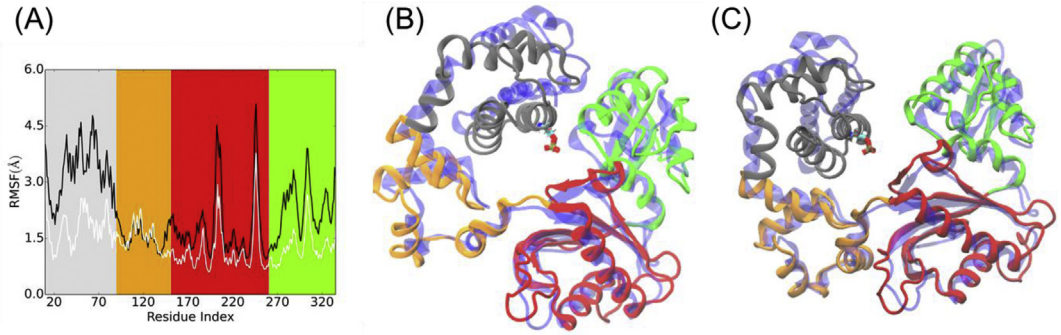

Fig. 3. (A) The Root Mean Squared Fluctuation (RMSF) for pS44-2FMS (black) compared with RMSF for apo-2FMS (white). The vertical panel colors reflect the DNA polymerase β major sub-domains are colored as follows: Lyase domain (grey) DNA binding (D) (orange), catalytic (C) (red), and nascent base pair binding (N) (green). (B) Structural alignment between apo_2FMS at the initial stage (Blue-Transparent) and average pS44-2FMS structure (sub-domain-colored) with phosphorylated S44 residue shown in bond representation. (C) Structural alignment between apo_3ISB at the initial stage (Blue-Transparent) and average pS44-2FMS structure (sub-domain-colored) with phosphorylated S44 residue shown in bond representation. (For interpretation of the references to color in this figure legend, the reader is referred to the Web version of this article.)

4.4. Salt bridges formed by pS44

In addition, to disrupting S44-E335 H-bond, phosphorylating S44 is expected to form new salt bridges with surrounding basic residues. We performed the salt bridge analysis for pS44-2FMS and S44D-2FMS systems. The results show that pS44 form is likely to form salt bridges with (R40, K41, K48, and R149) whereas S44D forms salt bridges with (R40, K41, and K48). The three first residues (R40, K41, and K48) lie within the Lyase domain with R149 located in the coil connecting the D-sub-domain to the C-sub-domain. Our simulations show that the formation of pS44-R149 salt bridge anti-correlates with the S44-E335 distance (Fig. 5A). The figure shows the pS44-R149 (O-N) distance anti-correlates with the S44-E335 distance indicating that the Lyase domain pS44-2FMS perform a large swing move between the N-sub-domain and R149 in the middle of the doughnut structure (Fig. 5B). Thus, the formation of these salt bridges is another contributing factor to the major conformational changes induced by pS44 in agreement with the results of [28].

The structural transformations induced by S44 phosphorylation can be also elucidated using cluster analysis. The results of this analysis are summarized in Table 2. The sampled conformations are clustered in three dominant structures. The first cluster with 38% dominance is characterized by a large S44-E335 distance (13.75 ± 2.176 Å), large RMSD value (5.02 ± 0.497 Å), and the possibility of forming the salt bridge between pS44 and R148. The other two clusters have smaller S44-E335 distances, smaller RMSD values, and don't form the pS44-R148 salt bridge. However, cluster 2 represents a more open structure more than cluster 3. In summary, the three clusters represent the shift of 2FMS structure from closed conformation (cluster 3) to open conformation (cluster 2) and to one where the Lyase domain swings toward the middle of the structure (cluster 1). This picture is consistent with Fig. 5.

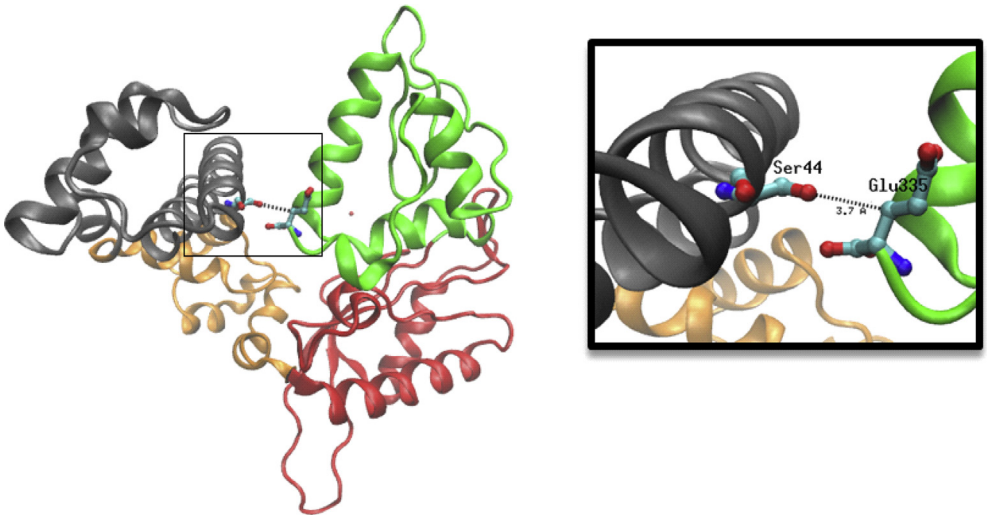

Fig. 4. The H-bond between S44 and E335 shown on the full apo-2FMS structure (left) and in the zoomed-up inset (right).

Table 1
The donor-acceptor distance between S44 and E335 (S44-E335 da) for five 2FMS and four 3ISB simulated systems. The second and third columns list the average and standard deviation values for S44-E335 length (da). The last column lists the average H-bond occupancy. The H-bond occupancy for 1BPD is shown as a reference point.

	S44-E335da avg (Å)	S44-E335da std (Å)	HB avg
2FMS			
apo	4.38	1.416	0.983
pS44	12.19	2.152	0.000
pS4455	10.85	2.252	0.000
pS55	5.24	2.001	0.530
S44D	8.85	1.714	0.00
3ISB			
apo	6.22	2.204	0.565
pS44	10.47	1.980	0.000
pS4455	10.61	1.938	0.000
pS55	5.48	3.213	0.817

5. Conclusion

Phosphorylation at S44 had induced major conformational fluctuation from apo_2FMS at the single strand DNA binding domain and dNTP selection domain. Adding a negative charge to S44 probably disrupts interactions between the lyase domain and the N-sub-domain of the polymerase (S44 and E335 H-bond in 2FMs). These conformation changes destabilize the closed structure. Thus the binding of single-strand DNA or dNTP might be affected by phosphorylation at these specific residues, causing DNA polymerase β′s failure to carry out its catalytic function (although the phosphorylated enzyme retained its DNA binding ability). Recent work by Su et al. [29] supports our conclusion that S44 phosphorylation exerts its effect on E335-S44 hydrogen bond. From experimental measurements, Su et al. implicate the amino acid cluster around E335 with control of opening and closure of dNTP binding cleft. Since our phosphorylation models show abolishment of the S44-E335 hydrogen bond, we argue that phosphorylation may abrogate the opening and closure of this binding cleft.

In their paper, Tokui et al. [7] were not able to infer whether phosphorylation of S44, S55 or both was responsible for the loss of the polymerase function. From our results, S44 phosphorylation seems responsible for inhibition of enzyme function *in vitro*, whilst S55 phosphorylation has the potential to aid the enzyme in catalysis by aiding in S44-E335 H-bond formation. Phosphorylation of the two serines could be mutually exclusive inside the cell, if it occurs, and may perform the aforementioned opposing functions. Our results can only be conclusively confirmed once the phosphorylated enzyme is crystallized and structures for the various phosphorylated variants solved.

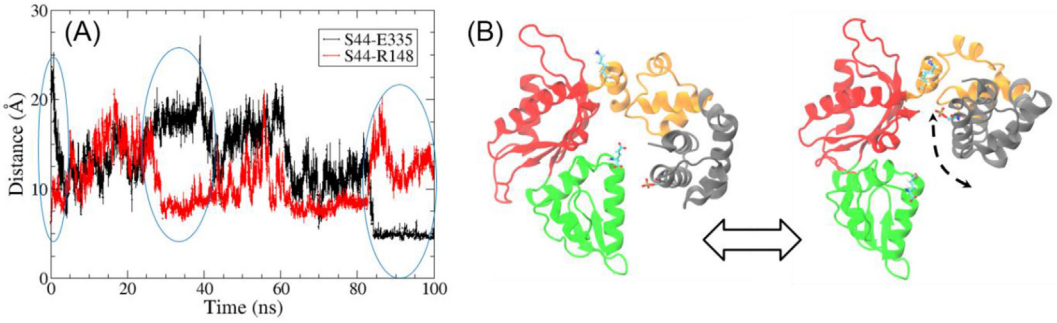

Fig. 5. (A) The pS44-E335 (black) and pS44-R148 (red) distances as a function of simulations time. The figure shows that these distances anti-correlate with each other over a large fraction of the time (highlighted in ovals). (B) Cartoon representation of pS44-2FMS swing move between a structure with small pS44-E335 distance (left) and a structure with small pS44-R148 distance which explains the anti-correlation in Fig. 5A. DNA polymerase β major sub-domains are colored as follows: Lyase domain (grey) DNA binding (D) (orange), catalytic (C) (red), and nascent base pair binding (N) (green). The residues pS44 (Lyase domain), R148 (D sub-domain), and E335 (N sub-domain) residues are shown in bond representation. (For interpretation of the references to color in this figure legend, the reader is referred to the Web version of this article.)

Table 2
The three dominant clusters of pS44-2FMS sampled conformations. Cluster 1 is the most dominant one with 38.0% frequency among all sampled conformations. The three clusters are characterized by the average values of RMSD, Rg, S44-E335 distance, S44-E335 donor/acceptor distance, and pS44-R148 salt bridge formation.

Cluster	Occupancy	RMSD (Å)	R_g (Å)	44-335 (Å)	44–335da (Å)	pS44-R148 salt bridge
1	38.0%	5.02	23.15	13.75	13.18	Yes
		0.497	0.781	2.176	1.447	
2	31.0%	3.47	23.42	9.88	9.46	No
		0.514	0.304	1.975	1.568	
3	31.0%	3.42	22.64	8.68	10.01	No
		0.596	0.366	1.352	1.648	

Acknowledgement

This project is a personal and voluntary initiative by Dr. Haitham Idriss in support of Palestinian science [30]. We thank Dr. William (Bill) A. Beard (NIEHS, NIH) for discussion and for supplying Fig. 4. NAMD simulations runs were performed in the 1200 cores HPC of Khalifa University. Dr. Haitham Idriss dedicates this work to the memory of his late brother Mr. Hisham Idriss (1952–2012). Dr. Haitham Idriss is grateful for his mother, Hajjah Mrs. Zahia Idriss (1929-2018), for her generous support during the course of this work.

Appendix A. Supplementary data

Supplementary data related to this article can be found at https://doi.org/10.1016/j.jmgm.2018.08.007.

References

[1] El-Khamisy, S.; Available from: https://recordings.join.me/QsbjemUlwESzukZiZVgypA.
[2] E. M Goellner, D. Svilar, K. H Almeida, R. W Sobol, Targeting DNA polymerase ss for therapeutic intervention, Curr. Mol. Pharmacol. 5 (1) (2012) 68–87.
[3] H.T. Idriss, O. Al-Assar, S.H. Wilson, DNA polymerase β, Int. J. Biochem. Cell Biol. 34 (4) (2002) 321–324.
[4] W.A. Beard, S.H. Wilson, Structure and mechanism of DNA polymerase β, Chem. Rev. 106 (2) (2006) 361–382.
[5] W.A. Beard, S.H. Wilson, Structure and mechanism of DNA polymerase β, Biochemistry 53 (17) (2014) 2768–2780.
[6] L. Kohlstaedt, J. Wang, J. Friedman, P. Rice, T. Steitz, Crystal structure at 3.5 angstrom resolution of HIV-1 reverse transcriptase complexed with an inhibitor, Science 256 (5065) (1992) 1783–1791.
[7] T. Tokui, M. Inagaki, K. Nishizawa, R. Yatani, M. Kusagawa, K. Ajiro, Y. Nishimoto, T. Date, A. Matsukage, Inactivation of DNA polymerase beta by in vitro phosphorylation with protein kinase C, J. Biol. Chem. 266 (17) (1991) 10820–10824.
[8] J. Fan, D.M. Wilson, Protein–protein interactions and posttranslational modifications in mammalian base excision repair, Free Radic. Biol. Med. 38 (9) (2005) 1121–1138.
[9] S. Hasan, N. El-Andaloussi, U. Hardeland, P.O. Hassa, C. Bürki, R. Imhof, P. Schär, M.O. Hottiger, Acetylation regulates the DNA end-trimming activity of DNA polymerase β, Mol. Cell 10 (5) (2002) 1213–1222.
[10] N. El-Andaloussi, T. Valovka, M. Toueille, R. Steinacher, F. Focke, P. Gehrig, M. Covic, P.O. Hassa, P. Schär, U. Hübscher, Arginine methylation regulates DNA polymerase β, Mol. Cell 22 (1) (2006) 51–62.
[11] L. Yang, K. Arora, W.A. Beard, S.H. Wilson, T. Schlick, Critical role of magnesium ions in DNA polymerase β's closing and active site assembly, J. Am. Chem. Soc. 126 (27) (2004) 8441–8453.
[12] Y. Li, C.L. Gridley, J. Jaeger, J.B. Sweasy, T. Schlick, Unfavorable electrostatic and steric interactions in DNA polymerase β E295K mutant interfere with the enzyme's pathway, J. Am. Chem. Soc. 134 (24) (2012) 9999.
[13] T. Schlick, K. Arora, W.A. Beard, S.H. Wilson, Perspective: pre-chemistry conformational changes in DNA polymerase mechanisms, Theor. Chem. Accounts 131 (12) (2012) 1287.
[14] V.K. Batra, W.A. Beard, D.D. Shock, J.M. Krahn, L.C. Pedersen, S.H. Wilson, Magnesium-induced assembly of a complete DNA polymerase catalytic complex, Structure 14 (4) (2006) 757–766.
[15] W.A. Beard, D.D. Shock, V.K. Batra, L.C. Pedersen, S.H. Wilson, DNA polymerase beta substrate specificity: side chain modulation of the "A-rule", J. Biol. Chem. 284 (46) (2009) 31680–31689.
[16] M.R. Sawaya, H. Pelletier, A. Kumar, S.H. Wilson, J. Kraut, Crystal structure of rat DNA polymerase beta: evidence for a common polymerase mechanism, Science 264 (5167) (1994) 1930–1935.
[17] W. Humphrey, A. Dalke, K. Schulten, VMD: visual molecular dynamics, J. Mol. Graph. 14 (1) (1996) 33–38.
[18] A.D. MacKerell Jr., D. Bashford, M. Bellott, R.L. Dunbrack Jr., J.D. Evanseck, M.J. Field, S. Fischer, J. Gao, H. Guo, S. Ha, All-atom empirical potential for molecular modeling and dynamics studies of proteins, J. Phys. Chem. B 102 (18) (1998) 3586–3616.
[19] G. Carpenter, S. Grossberg, ART2: Self-organization of Stable Category Recognition Codes for Analog Input Patterns, vol 1991, US Army Research Office, 1987.
[20] M.E. Karpen, D.J. Tobias, C. Brooks 3rd, Statistical clustering techniques for the analysis of long molecular dynamics trajectories: analysis of 2.2-ns trajectories of YPGDV, Biochemistry 32 (2) (1993) 412–420.
[21] Z. Guo, D. Thirumalai, The nucleation-collapse mechanism in protein folding: evidence for the non-uniqueness of the folding nucleus, Folding Des. 2 (6) (1997) 377–391.
[22] W. Kabsch, C. Sander, Dictionary of protein secondary structure: pattern recognition of hydrogen-bonded and geometrical features, Biopolymers 22 (12) (1983) 2577–2637.
[23] J.C. Phillips, R. Braun, W. Wang, J. Gumbart, E. Tajkhorshid, E. Villa, C. Chipot, R.D. Skeel, L. Kale, K. Schulten, Scalable molecular dynamics with NAMD, J. Comput. Chem. 26 (16) (2005) 1781–1802.
[24] W.L. Jorgensen, J. Chandrasekhar, J.D. Madura, R.W. Impey, M.L. Klein, Comparison of simple potential functions for simulating liquid water, J. Chem. Phys. 79 (2) (1983) 926–935.
[25] G.J. Martyna, D.J. Tobias, M.L. Klein, Constant pressure molecular dynamics algorithms, J. Chem. Phys. 101 (5) (1994) 4177–4189.
[26] T. Darden, D. York, L. Pedersen, Particle mesh Ewald: an N· log (N) method for Ewald sums in large systems, J. Chem. Phys. 98 (12) (1993) 10089–10092.
[27] U. Essmann, L. Perera, M.L. Berkowitz, T. Darden, H. Lee, L.G. Pedersen, A smooth particle mesh Ewald method, J. Chem. Phys. 103 (19) (1995) 8577–8593.
[28] D.J. Mandell, I. Chorny, E.S. Groban, S.E. Wong, E. Levine, C.S. Rapp, M.P. Jacobson, Strengths of hydrogen bonds involving phosphorylated amino acid side chains, J. Am. Chem. Soc. 129 (4) (2007) 820–827.
[29] J.G. Su, X. Jin Xu, C. Hua Li, W.Z. Chen, C.X. Wang, Identification of key residues for protein conformational transition using elastic network model, J. Chem. Phys. 135 (17) (2011) 11B601.
[30] G.O. Tadmouri, Biomedical bibliometrics of a country with multiple identities;the case of Palestine, Ann. Alquds Med. 2 (2006) 63–68.